Dalton Transactions

Accepted Manuscript

ROYAL SOCIETY OF CHEMISTRY

rsc.li/dalton

View Article Online
DOI: 10.1039/C6DT03521C

Dalton Transactions

PAPER

Nanostructured discotic Pd(II) metallomesogens as one-dimensional proton conductors

Received 00th January 20xx,
Accepted 00th January 20xx

DOI: 10.1039/x0xx00000x

www.rsc.org/

Cristián Cuerva,[a] José A. Campo,[a] Mercedes Cano*[a] and Rainer Schmidt*[b]

A novel family of square-planar Pd(II) complexes based on isoquinoline-functionalised pyrazolate ligands $[Pd(pz^{R(n,n)iq})_2]$ (R(n,n) = $C_6H_3(OC_nH_{2n+1})_2$, n = 4, 6, 8, 10, 12, 14, 16, 18) have been synthesised and characterised. The new complexes show mesomorphic properties and exhibit columnar mesophases that are highly-stable in exceptionally wide temperature ranges of up to 345 ºC. The formation of nanochannels in the fluid liquid crystal phases generates continuous pathways for one-dimensional proton conduction on the basis of a C-H···N proton transfer. The complex with an intermediate chain length (n = 12) shows the highest proton conductivity of 1.34 x 10^{-4} S m^{-1} at 269 ºC in the hexagonal columnar mesophase, and an activation energy of 0.84 eV. The influence of both the terminal alkyl chain length and the mesophase columnar organisation on the proton conduction mechanism is demonstrated. The series of Pd(II) complexes investigated in this work constitutes one of the first examples of proton-conducting metallomesogens with potential applications in PEM fuel cells.

Introduction

Discotic liquid crystals (DLCs) are a class of nanomaterials that have attracted great interest due to their application in optoelectronic devices.[1, 2] The columnar arrangement of the disc-like molecules can be used as a support to favour one-dimensional electron and hole transport, as expected for a 1D semiconductor.[3-5] It was in 1993 that for the first time electronic conduction in the hexagonal columnar mesophase of an organic DLC was explored,[6] and a few years later, an organic photovoltaic device incorporating this type of materials was reported.[7] Since then, a great variety of organic liquid crystals with an aromatic core and several terminal alkyl chains have been described to be useful as active components in light-emitting diodes,[8-10] field effect transistors[11-13] and solar cells.[14-17] The effective charge transport along the central π-system of DLCs was established to be the key factor for highly-efficient devices.

On the other hand, DLCs are also promising candidates for the transport of ions.[18-21] The use of the nanochannels present in the columnar mesophase to achieve continuous pathways for ion conduction can be considered of high interest in the development of new batteries and fuel cells. In this context, self-organised ionic liquid crystals have been found to exhibit anisotropic ionic conductivity,[18] whereas more recently zwitterionic liquid crystals without transportable ions could be strategically modified by doping them with lithium salts in order to establish Li ion conduction.[22] It was also demonstrated that the fluid state of the mesophase favours ion conduction at low temperatures even in a water-free medium, which would increase the operational temperature range of conventional water-based fuel cells.

Recently, progress has been made on the design of proton-conducting liquid crystals that are self-assembled with protic salts or functionalised with acidic groups for potential application in proton exchange membrane (PEM) fuel cells.[23-25] It has been reported that columnar mesophases clearly decrease the activation energy necessary for proton conduction to occur.[25] However, from the best of our knowledge only some few materials with these characteristics have been described in the literature and in most cases certain humidity conditions are required for efficient proton transport.[23-27]

Over the last years, we have been working on dicatenar pyridylpyrazolate Pd(II) and Pt(II) complexes which behave as liquid crystal materials exhibiting hexagonal columnar mesophases.[28-30] The high planarity of the pyrazolate core favours the π-stacking of disc-like molecules, which are self-assembled in a hexagonal lattice forming nanochannels in the mesophase. Recently, we have reported a new family of isoquinoline-functionalised pyrazolate Pt(II) complexes $[Pt(pz^{R(n,n)iq})_2]$ based on 3-(3,5-bis(alkyloxy)phenyl)-5-(isoquinolin-3-yl)pyrazolate ligands, $pz^{R(n,n)iq}$ (R(n,n) = $C_6H_3(OC_nH_{2n+1})_2$, n = 4, 6, 8, 10, 12, 14, 16, 18), which exhibit tetragonal and hexagonal columnar mesophases.[31] In

[a] Departamento de Química Inorgánica I, Facultad de Ciencias Químicas, Universidad Complutense de Madrid, Ciudad Universitaria, E-28040 Madrid, Spain. E-mail: mmcano@ucm.es; Fax: +34-91394-4352; Tel: +34-91394-4340.
[b] GFMC. Departamento de Física Aplicada III, Universidad Complutense de Madrid, Ciudad Universitaria, E-28040 Madrid, Spain. E-mail: rainerxschmidt@googlemail.com.

† Electronic Supplementary Information (ESI) available: POM microphotographs, DSC curves, TG-DTG curves, -Z'' vs Z' plots, C' vs T plots and σ' vs T plots. See DOI: 10.1039/x0xx00000x

View Article Online
DOI: 10.1039/C6DT03521C

comparison with the analogous bis(pyridylpyrazolate)platinum(II) liquid crystals previously reported,[29] the presence of the isoquinoline moiety has allowed to increase the temperature range of existence of the mesophase. Although these metallomesogens have shown interesting applications such as temperature sensors, however, the high temperatures reached produced a partial degradation of the samples in the mesophase which would restrict some of their potential applications.

Encouraged by our previous results, we were interested in improving the thermal stability of this type of liquid crystals, and then in obtaining novel materials that can be used for potential application as proton exchange membranes by using the nanochannels found in the mesophase. In this context, a wider temperature range of existence of the mesophase gives access to ionic conductivities at elevated operating temperatures to overcome the current limit of PEM fuel cells. Following this idea, here in this work we report on a new family of isoquinolinylpyrazolate Pd(II) complexes of the type $[Pd(pz^{R(n,n)iq})_2]$. In all cases, the decomposition temperatures are close to the high clearing ones, and the complexes exhibit highly-stable mesophases over exceptionally wide temperature ranges. The high thermal and mechanical stability of these liquid crystals, in combination with the presence of nanochannels in the mesophase, has allowed the development of a new class of water-free proton conductors. The electrical properties have been examined by complex impedance spectroscopy to investigate the influence of the terminal alkyl chain length and to generally assess the potential for PEM applications in the mesophase.

Results and Discussion

Synthesis and structural characterisation

The synthetic route to prepare the new bispyrazolate Pd(II) complexes $[Pd(pz^{R(n,n)iq})_2]$ (compounds **1** - **8**) is depicted in Scheme 1. Dicatenar isoquinoline-functionalised pyrazoles were synthesised through a Claisen condensation between the corresponding 3,5-*n*-dialkyloxyacetophenone and ethyl isoquinoline-3-carboxylate, followed by treatment with hydrazine monohydrate.[31] The reactions of these derivatives with palladium(II) acetate in a 1 : 2 (metal:ligand) molar ratio and basic conditions result in the new palladium complexes in good yields (40 - 60%). All of them were isolated as stable yellow solids at room temperature.

The Pd(II) complexes were fully characterised by infrared (IR), 1D and 2D nuclear magnetic resonance (NMR) spectroscopies and CHN elemental analyses.

The IR spectra in the solid state show the characteristic ν(C=N) and ν(C=C) bands of the isoquinoline and pyrazolate groups at 1637-1595 cm^{-1}, as well as those associated with the symmetric and antisymmetric stretches of the alkyl chains at around 2900 cm^{-1}. The ν(C=N) and ν(C=C) bands are slightly higher in energy to that reported for the free isoquinolinylpyrazole ligands as a consequence of the

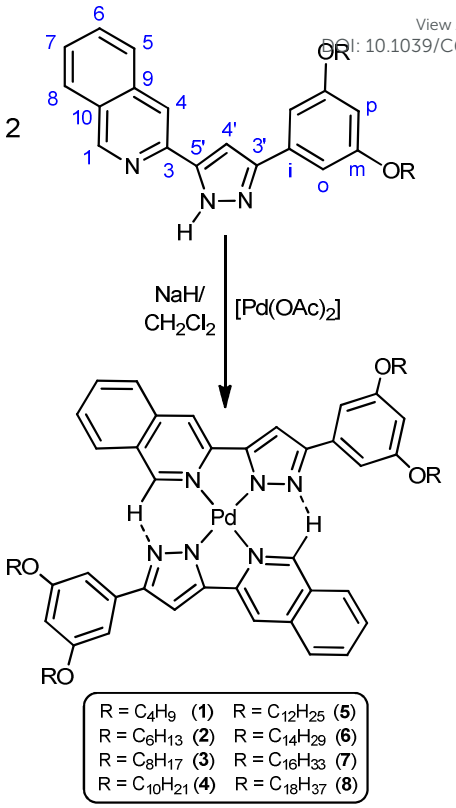

Scheme 1 Synthesis of the Pd(II) complexes $[Pd(pz^{R(n,n)iq})_2]$ (**1**-**8**). The atom numbering showed in the ligand structure is used for NMR assignments.

coordination to the metal centre.[31] Moreover, the anionic nature of the coordinated ligands is confirmed by the absence of ν(N-H) vibrations in the highest-energy region (see experimental section).

The ^{1}H NMR spectra of all complexes in $CDCl_3$ solution at room temperature display the typical signals of the pyrazole core as well as those of the isoquinolinyl and alkyloxyphenyl aromatic substituents. In agreement with the overall equivalence of the two pyrazolate ligands around the metal centre only a unique set of signals was observed for each type of protons. A combination of 2D COSY and selective 1D NOESY spectra were required for the assignment of all resonances (see experimental section for a summary of all NMR data). It is noteworthy that the signal corresponding to 1-H protons at around 10.5 ppm is down-field shifted with respect to that of the free ligands (*ca.* 9.3 ppm).[31] This feature, together with the absence of NH signal resonances, is consistent with the anionic nature of the coordinated ligands and the formation of intramolecular C–H···N hydrogen bonds in solution, as it has been previously reported for analogous bispyrazolate complexes.[28, 29, 31-34]

Additionally, the ^{13}C NMR spectrum of compound **3** was also recorded in $CDCl_3$ solution (~ 0.3 M) at room temperature. DEPT and 2D ^{1}H–^{13}C HMQC and ^{1}H–^{13}C HMBC NMR experiments were carried out for a full interpretation of the ^{13}C NMR spectrum. All signals are consistent with the proposed formulation (see experimental section for more details).

Table 1 Phase transitions of Pd(II) complexes $[Pd(pz^{R(n,n)iq})_2]$ (**1**-**8**).

Compound	Transitions[a]	T[b] [ºC] (ΔH/kJ mol^{-1})	T_{dec}[d] [ºC]
1	Cr→Col_t→Col_h→I	155 (36.8), 228 (26.9), 440	430
	I→Col_h→Cr	360, 108	
2	Cr→Col_h→I	98 (43.6), 447	405
	I→Col_h→Cr	361, 87	
3	Cr→Col_h→I	112 (54.1), 436	401
	I→Col_h→Cr	350, 25[c]	
4	Cr→Col_h→I	105 (63.5), 424	370
	I→Col_h→Cr	390, 25[c]	
5	Cr→Col_h→I	91 (64.7), 385	370
	I→Col_h→Cr	374, 25[c]	
6	Cr→Col_h→I	99 (93.7), 389	420
	I→Col_h→Cr	385, 25[c]	
7	Cr→Cr'→Col_h→I	52 (47.7), 98 (22.3), 344	390
	I→Col_h→Cr	334, 25[c]	
8	Cr→Cr'→Col_h→I	64 (113.8), 96 (13.4), 355	393
	I→Col_h→Cr	351, 25[c]	

[a] Cr, Cr' = crystalline phase, Col_t = tetragonal columnar mesophase, Col_h = hexagonal columnar mesophase, I = isotropic liquid; [b] Enthalpies of the Col_h→I, I→Col_h and Col_h→Cr phase transitions were not determined due to partial decomposition and the corresponding temperatures are given by POM; [c] The liquid crystal phase remains metastable for several hours. [d] Decomposition temperature T_{dec}, defined as the temperature where a 5% weight loss has occurred.

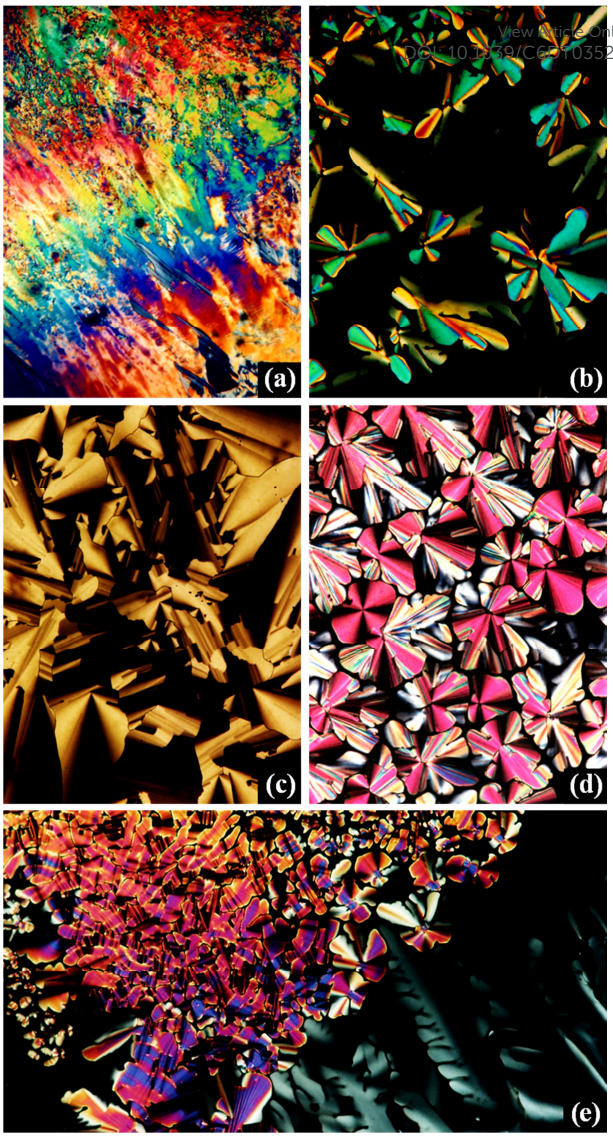

Fig. 1 POM microphotographs of the Col_h mesophase of **(a)** $[Pd(pz^{R(8,8)iq})_2]$ **3** at 291 ºC on heating, **(b)** $[Pd(pz^{R(8,8)iq})_2]$ **3** at 249 ºC on cooling, **(c)** $[Pd(pz^{R(16,16)iq})_2]$ **7** at 335 ºC on cooling, **(d)** $[Pd(pz^{R(6,6)iq})_2]$ **2** at 129 ºC on cooling and **(e)** $[Pd(pz^{R(18,18)iq})_2]$ **8** at 204 ºC on cooling.

Mesomorphism

All Pd(II) complexes (compounds **1** – **8**) show enantiotropic liquid crystal properties in a very wide temperature interval. The thermal behaviour was studied by polarised light optical microscopy (POM), differential scanning calorimetry (DSC), thermogravimetric analysis (TGA) and powder X-ray diffraction (XRD) at variable temperature. The phase transition temperatures and their associated enthalpy data are summarised in Table 1.

By heating the compounds **2** - **8** under polarised light, all crystalline solid phases are consistently transformed at the melting point of around 100 ºC into liquid crystal phases which exhibit a birefringent texture with a high mobility (Fig. 1a and S1†). In agreement with the POM observations, the DSC thermograms show an endothermic peak around 100 ºC that can be attributed to this solid-mesophase transition (see Fig. S2†). The molecular arrangement in the mesophase was confirmed to be hexagonal columnar (Col_h) from X-ray data presented at the end of this section. An additional peak at *ca.* 50 - 60 ºC is observed for compounds **7** and **8**, which agrees with the existence of a solid-solid phase transition (Fig. S2†).

Curiously, complex **1** with the shortest alkyl chains exhibits a different thermal behaviour: by heating across 155 ºC the crystalline solid (Cr) transforms into a tetragonal columnar mesophase (Col_t) with a birefringent and viscous texture, which is then transformed later at 228 ºC into a hexagonal columnar mesophase (Col_h) with a lower viscosity. Both phase transitions could be clearly identified in the DSC trace of **1** (see Table 1 and Fig. S2†).

By further heating the Col_h mesophase of all complexes transform into a liquid phase at the clearing temperature. Here we find exceptionally high values of 344 to 447 ºC, which implies a high stability of the liquid crystalline phase. The compounds **6** - **8** start to decompose at T_{dec} between 390 – 420 ºC (see Table 1 and Fig. S3†). On the other hand, compounds **1** - **5** already start to decompose in the mesophase between 370 ºC – 430 ºC below the clearing point of the respective complexes.

For conventional POM observations, the complexes were heated up just to the clearing point into the liquid isotropic phase, followed by cooling to room temperature. For

DOI: 10.1039/C6DT03521C

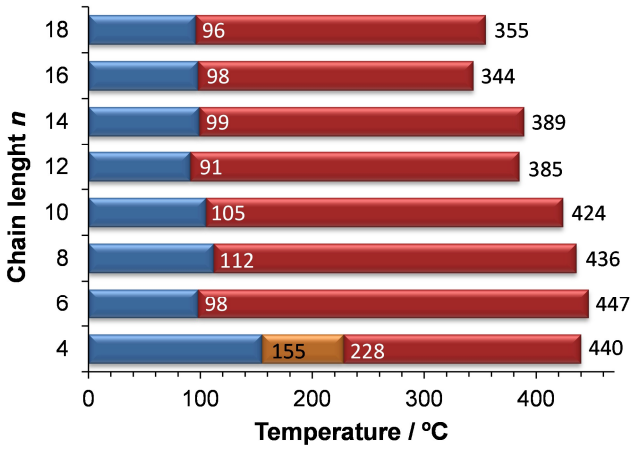

Fig. 2 Bar diagram representing the melting and clearing temperatures of the Pd(II) metallomesogens.

compounds **1** - **5** the decomposition temperature T_{dec} is below the clearing temperature as it has been already mentioned, leading to the partial decomposition. However, the temperature was held above the clearing point for a very short time only (*ca*. 10 sec.), and so that we ensure that sufficiently large areas retain the mesophase features to clearly visualise them in the POM micrographs upon cooling (Fig. 1b-e). In all cases, the Pd(II) complexes display the typical dendritic and pseudo focal-conic textures of a columnar mesophase. Homeotropic domains (dark areas in Fig. 1b,e) are observed even at high cooling rates, which evidence the preferable face-on alignment of the disc-like molecules.[35, 36] With the exception of compounds **1** and **2**, the mesophase remains metastable for several hours after cooling to room temperature due to a slow solidification process. Thus, the exothermic peak corresponding to the mesophase-solid phase transition on cooling could not be detected in the DSC thermograms.

Fig. 2 shows a bar diagram comparing the temperatures of the phase transitions for these Pd(II) complexes. The melting point of all complexes is found to be rather similar regardless of the alkyl chains length (with the exception of **1**). On the other hand, the clearing temperatures generally decrease with increasing the number of carbon atoms at the terminal chains, which can be explained by a higher mobility that hinders the establishment of intermolecular interactions in the mesophase.

The above results are consistent with those reported for the analogous isoquinolinylpyrazolate Pt(II) complexes.[31] The melting temperatures are similar (*ca*. 100 ºC) and the clearing points are slightly lower for the new palladium derivatives, which also exhibit higher decomposition temperatures. Thus, the mesophase of the Pd(II) derivatives is practically stable in the overall range of existence. On the other hand, the temperature range of the mesophases is notably higher than that of related Pd(II) and Pt(II) complexes bearing pyridylpyrazolate ligands. It demonstrates that the isoquinoline group improves the thermal stability of the mesophase, and therefore the liquid crystal properties of the new metal complexes.

Table 2 XRD data for Pd(II) compounds **1**, **5**, **7** and **8**

	Phase	2ϑ [º]	d_{meas} [a] [Å]	d_{calc} [a] [Å]	[*hkl*] [b]	Parameters [c]
1	Col_t	5.8	15.3	15.3	100	T = 170 ºC
		8.2	10.8	10.8	110	a = 15.3 Å
		11.5	7.7	7.7	200	S_{col} = 234 Å^2
		12.8	6.9	6.8	210	
		16.8	5.3	5.4	220	
		17.7	5.0	5.1	300	
		18.2	4.9	4.8	310	
		20.4	4.3	4.2	230	
		23.1	3.8	3.7	140	
	Col_h	4.9	17.9	17.9	100	T = 230 ºC
		8.5	10.4	10.3	110	a = 20.9 Å
		9.8	9.1	9.0	200	V_{mol} = 1295 Å^3
		12.9	6.9	6.8	210	S_{col} = 378 Å^2
		17.0	5.2	-	-	h = 3.4 Å
		25.9	3.4	-	001	
5	Col_h	3.8	23.0	23.0	100	T = 110 ºC
		6.6	13.5	13.3	110	a = 26.9 Å
		7.6	11.7	11.5	200	V_{mol} = 2089 Å^3
		10.0	8.8	8.7	210	S_{col} = 627 Å^2
		18.0	4.9	-	-	h = 3.3 Å
		26.4	3.4	-	001	
7	Col_h	3.4	26.0	26.0	100	T = 100 ºC
		5.9	15.1	15.0	110	a = 30.2 Å
		6.8	13.1	13.0	200	V_{mol} = 2671 Å^3
		18.0	4.9	-	-	S_{col} = 790 Å^2
		26.2	3.4	-	001	h = 3.4 Å
8	Col_h	3.3	27.1	27.1	100	T = 120 ºC
		5.6	15.9	15.7	110	a = 31.5 Å
		6.5	13.6	13.6	200	V_{mol} = 2858 Å^3
		18.0	4.9	-	-	S_{col} = 859 Å^2
		26.2	3.4	-	001	h = 3.3 Å

[a] d_{meas} and d_{calc} are the measured and calculated diffraction spacings; [b] [*hkl*] are the Miller indices of the reflections; [c] Molecular volume: $V_{mol} = M_w/(N_A \cdot \rho)$; where M_w is the molecular weight, N_A is Avogadro's number and ρ is the density (~ 1.0-1.2 g·cm^{-3}). For tetragonal columnar phases: lattice constant $a = d_{100}$; columnar cross-section area $S_{col} = a^2$. For hexagonal columnar phases: lattice constant $a = 2[\Sigma d_{hk}\sqrt{(h^2 + k^2 + hk)}]/\sqrt{3}N_{hk}$, where N_{hk} is the number of *hk0* reflections; columnar cross-section area $S_{col} = (\sqrt{3})a^2/2$; intracolumnar distance $h = V_{mol}/S_{col}$.

The type of columnar ordering in the mesophase was established from powder X-ray diffraction experiments at variable temperature. Calculated values of Bragg's spacing ($d_{calc.}$) were obtained from the reciprocal spacing ratio characteristic for tetragonal and hexagonal symmetries, assigning the first peak observed to the (100) reflection. Compounds **1**, **5**, **7** and **8** were selected as representative examples and the results are summarised in Table 2.

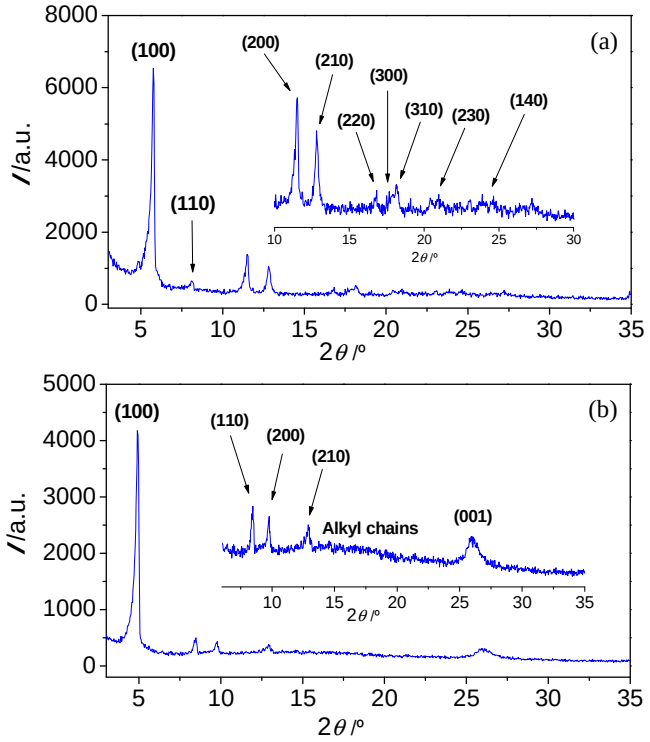

Fig. 3 Powder XRD diffraction patterns for complex [Pd(pz$^{R(4,4)iq}$)$_2$] **1** in **(a)** the tetragonal columnar mesophase (Col$_t$) and in **(b)** the hexagonal columnar mesophase (Col$_h$).

The XRD patterns of compound **1** clearly show the formation of the two different arrangements in the liquid crystal state (Fig. 3). Diffractograms recorded between 150 ºC and 210 ºC display well-resolved peaks with a *d*-spacing ratio of 1 : 1/√2 : 1/√4 : 1/√5 : 1/√8 : 1/√9 : 1/√10 : 1/√13 : 1/√17 which can be attributed to a tetragonal mesophase. By contrast, the characteristic (100), (110), (200) and (210) reflections of a hexagonal mesophase are observed at temperatures above 230 ºC with a *d*-spacing ratio of 1 : 1/√3 : 1/√4 : 1/√7. The tetragonal columnar mesophase is not frequently found and only some few liquid crystals with this arrangement have been reported to date.[37-39]

For compounds **5**, **7** and **8**, the XRD diffractograms show the (100), (110) and (200) reflections of a Col$_h$ mesophase at temperatures above the melting point, followed by a diffuse halo attributed to the liquid-like order of the molten alkyl chains (*ca*. 18º). Particularly for **5**, the (210) reflection is also observed. The stacking or intracolumnar distance *h* obtained from the (001) reflection was 3.4 Å in all cases, which is a value that is consistent with the relationship between the molecular volume and the columnar cross-section area of these complexes (see Table 2). Additionally, the solid-solid phase transitions of **7** and **8** could be observed at low temperatures in agreement with the DSC data described above.

Proton conductivity measurements

The ionic conductivities and dielectric properties of the representative compounds **1**, **2**, **4**, **5** and **7** were studied in the solid state and in the mesophase, whereas the high temperature liquid state was not accessible experimentally.

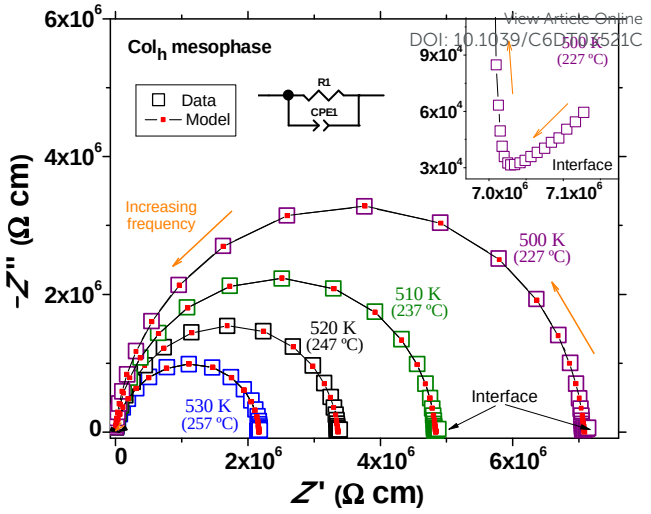

Fig. 4 -*Z*'' vs *Z*' plots for the complex [Pd(pz$^{R(12,12)iq}$)$_2$] **5** in the Col$_h$ mesophase at 500 K (227 ºC), 510 K (237 ºC), 520 K (247 ºC) and 530 K (257 ºC). Open squares represent measured data and solid lines with squares display equivalent circuit fits obtained by using the model depicted in the figure. The inset shows the details of the interface pike for the data collected at 500 K (227 ºC).

Fig. 4 displays an impedance plane plot of imaginary vs real part of the impedance -Z'' vs Z' collected in the mesophase of compound **5** at 500 K (227 ºC), 510 K (237 ºC), 520 K (247 ºC) and 530 K (257 ºC). The presence of a single semicircle at each temperature indicates that the dielectric contribution of the Pd(II) complex exhibits a single dielectric relaxation time τ, and thus the data can be modelled by one non-ideal resistor-capacitor (RC) element (see Fig. 4). The finding of a single τ implies that the ionic charge transport mechanism may be rather uniform along the nanochannels formed by the ordered molecules, whereas inter-channel transfers or other contributions would be expected to exhibit different τ. This would be manifested by the occurrence of additional semicircles,[40, 41] which is not what we observe. This behaviour is confirmed in all other Pd(II) complexes investigated (see Supporting Information, Fig. S4†).

The ideal capacitor in the standard RC element (in Fig. 4) has been replaced by a constant phase element (CPE), which accounts for the non-ideality of the respective dielectric contribution. On a microscopic level, the CPE behaviour is usually explained in the framework of a jump-relaxation of the ionic carriers at high frequency (*f*),[42] or alternatively by a broadening of the distribution of characteristic dielectric relaxation times τ across the sample.[43]

The resistivity ρ of the ionic charge transport is determined by the semicircle diameter, which decreases by increasing the temperature in accordance with the typical thermal activation of ionic charge transport.[44-46] In fact, an additional dielectric contribution with a pike-like shape is observed at low frequencies (Fig. 4 inset), which is a hall-mark feature of ionic conductors and diffusive type charge transport across the interface between the complexes and the metallic electrodes.[47, 48] The ionic conduction in this type of complexes has been recently reported to originate from a novel C-H···N proton transfer.[49] Accordingly, the pike-like contribution

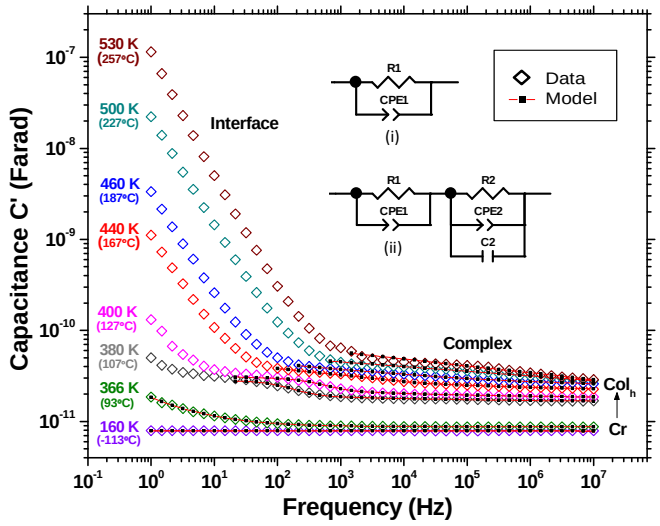

Fig. 5 *C*' vs *f* plots for the complex [Pd(pz$^{R(12,12)iq}$)$_2$] **5** at selected temperatures. Open squares represent measured data and solid lines with squares display equivalent circuit fits obtained by using the model (i) for the temperature ranges: 160-366 K (-113 – 93 ºC) and 440 – 530 K (167 – 257 ºC), and (ii) for 380 – 400 K (107 – 127 ºC).

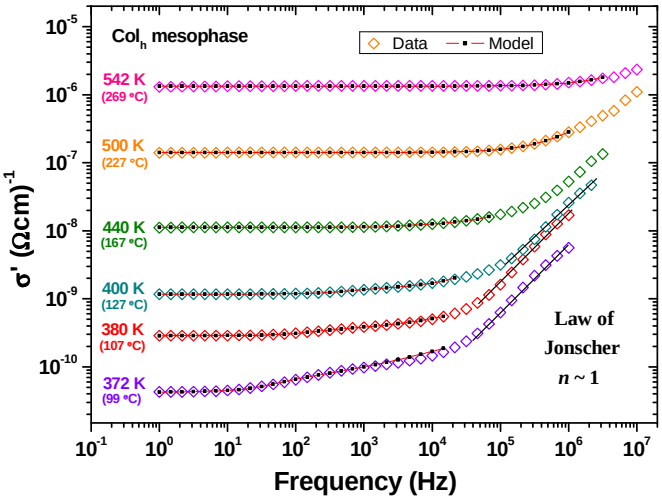

Fig. 6 σ' vs *f* plots for the complex [Pd(pz$^{R(12,12)iq}$)$_2$] **5** in the Col$_h$ mesophase at selected temperatures. Open squares represent measured data and solid lines with squares display equivalent circuit fits.

evidences that the conventional motion of protons is blocked at the interface regions and, therefore, we can confirm that no electronic charge carriers significantly contribute to the conduction.

The dielectric data were also plotted in the format of capacitance *C*' vs *f* in order to further corroborate the ionic nature of the predominant charge carriers. The temperature dependence of *C*' vs *f* curves for compound **5** upon heating is depicted in Fig. 5. Notably, the solid-mesophase phase transition (Cr → Col$_h$) is clearly reflected by an abrupt increase in the approximately *f*-independent plateau at intermediate and high *f*. The linear and continuous increase of *C*' with decreasing *f* is another hall-mark feature of ionic conductivity and can also be attributed to the charge blocking at the electrode interfaces.[47]

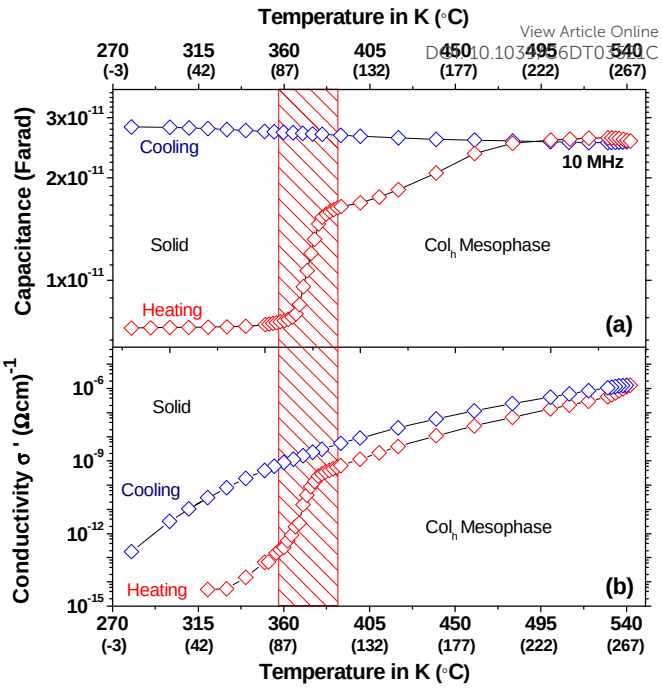

Fig. 7 (a) *C*' vs *T* plots measured at 10 mHz and (b) *s*' vs *T* plots from equivalent circuit fits for the complex [Pd(pz$^{R(12,12)iq}$)$_2$] **5** at selected temperatures in a heating-cooling cycle. The red shaded area shows the Cr-Col$_h$ phase transition on heating.

Furthermore, the real part of conductivity σ' vs *f* for the representative Pd(II) compound **5** is displayed in Fig. 6 at selected temperatures in the mesophase. The intrinsic protonic conductivity of the complex is observed in form of a thermally Arrhenius activated plateau at low and intermediate frequencies. At lower temperatures of 372 – 400 K (99 – 127 ºC) in the Col$_h$ mesophase, a second and rather small conductivity plateau appears at intermediate *f*, in agreement with the *C*' vs *f* data in Fig. 5. This feature is again typical for ionic conductors and was accounted for by an additional series R-CPE-C element in the equivalent circuit model used to fit the experimental values at these particular temperatures.

At high *f*, the σ' vs *f* curves show an up-turn, where the data at 380 K and 400 K in the Col$_h$ mesophase fall approximately on one single line with a constant gradient. This can be interpreted in terms of Jonscher's universal dielectric response law with a critical Jonscher exponent of $n \approx 1$. Although values of *n* greater than one have been reported for protonic conductors with energetically unfavourable ion acceptor sites, the typical power law exponent is usually found to be $n < 1$.[50]

Further information can be obtained from the plots of the capacitance and conductivity values extracted from the equivalent circuit fits as a function of the temperature, shown in Fig. 7 for compound **5**. Complementing our POM and DSC data shown above, the melting point is manifested by an abrupt change in both the *C*' and σ' vs *T* curves at the transition temperature of ≈ 90 ºC. The capacitance is maintained upon cooling at the maximum value reached in the liquid-crystalline state. By contrast, the conductivity decreases with decreasing temperature and the heat treated Pd(II)

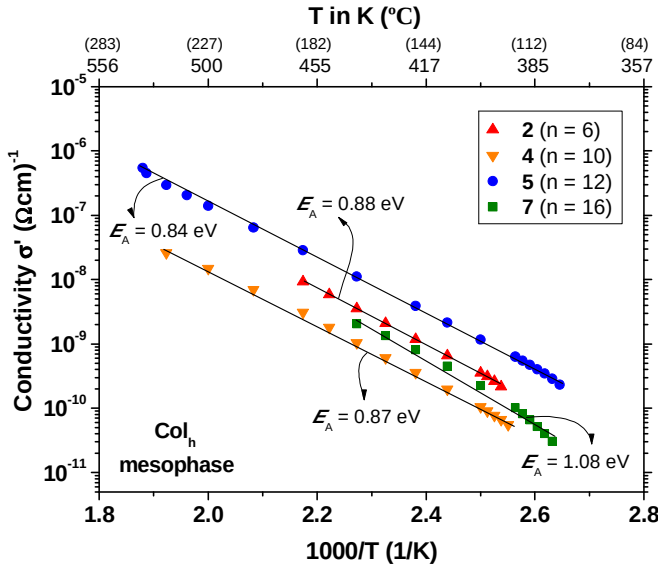

Fig. 8 σ' vs 1000/T plots extracted from equivalent circuit fits for the Pd(II) complexes $[Pd(pz^{R(n,n)iq})_2]$ **2**, **4**, **5**, **7** in the hexagonal columnar mesophase upon heating.

complex is less insulating at room temperature than the starting material.

In general terms, the dielectric behaviour is similar in all Pd(II) metallomesogens analysed (Fig. S5-S8†). Slight differences were detected in the shortest butyloxy derivative **1**, which exhibits two mesophases upon heating (see Table 1) that are clearly reflected in the intrinsic capacitance and conductivity of the metallomesogen (see Fig. S5†). It is indicated that the Col_h mesophase may be more favourable for proton conduction than the Col_t arrangement at lower temperatures, because σ' increases by heating across the Col_t-Col_h transition.

As mentioned above, compound **7** undergoes a solid-solid phase transition at temperatures near to the melting point (see Table 1), which produces a slight increase of both the capacitance and conductivity properties (Fig. S8†). Most likely, the supramolecular organisation of the new solid is similar to that of the Col_h mesophase and therefore, the potential presence of nanochannels may already facilitate the protonic charge transport.

The protonic conductivity was compared between the different complexes analysed (**1**, **2**, **4**, **5**, **7**) by using the σ' values extracted from equivalent circuit fits (Fig. 7 and S5-S8†). Interestingly, the complex with an intermediate chain length (**5**) exhibits the highest conductivity of 1.34 μS cm^{-1} at 542 K (269 ºC), followed by the compound **7** with a maximum value of ≈ 1.0 μS cm^{-1}. This feature can be understood by keeping in mind that complexes with shorter alkyl chains exhibit less fluidity, which may lead to reduced cooperative motions of the molecules by axial fluctuations. Thus, the mean effective hopping distance in these derivatives would be higher than that of the analogous complexes with longer terminal chains as it has been argued previously,[49] and therefore a decrease in conductivity would be expected. Also note that the longer alkyl chains can restrict the cooperative motions of the molecules by steric effects, which would explain that the conductivity for **7** is slightly lower than that found for the compound **5**.

The activation energies E_A in the mesophase were obtained from the corresponding Arrhenius plots of $\ln\sigma_{dc}$ vs $1/T$ and they are found to be in the range of 0.84 - 1.08 eV for compounds **2**, **4**, **5** and **7** (Fig. 8). E_A relates to the energy barrier that ionic charge carriers have to overcome to complete the transfer from a donor to an acceptor site, where the E_A values detected here may be considered typical values for ionically conducting materials.[51, 52] It is interesting to note that the E_A of compound **1** in the Col_t mesophase is 3.86 eV, while that determined in the Col_h one is only 0.50 eV. The low value of 0.50 eV thus indicates a lower energy barrier for a proton transfer to occur. This demonstrates that the Col_h organisation in the liquid crystal state of **1** clearly favours proton conduction, confirming our above arguments from σ' vs T plots.

By comparing the dielectric properties of these new metallomesogens with those of related pyridylpyrazolate Pd(II) complexes previously reported,[49] we can conclude that in both series of complexes the highest conductivity in the mesophase has been found for derivatives with 12 carbon atoms at the terminal alkyl chains. Moreover, the conductivity value σ' of compound **5** (σ' = 3.90 x 10^{-9} S cm^{-1} at 420 K (147 ºC)) is similar to that of the previously reported analogous Pd(II) complex, $[Pd(pz^{R(12,12)py})_2]$ ("PD12") (σ' = 2.43 x 10^{-9} S cm^{-1} at 420 K (147 ºC)).[49] However, the compound **5** exhibits a maximum conductivity value in the mesophase of 1.34 x 10^{-6} S cm^{-1} at 542 K (269 ºC), whereas the highest accessible conductivity of "PD12" was 4.62 x 10^{-8} S cm^{-1} at 450 K (177 ºC). This evidences that the improved operational temperature range for proton conduction gives access to considerably higher proton conductivities, which is a promising result in the search of novel metallomesogenic materials with high thermal and mechanical stability for potential applications as electrolytes.

Conclusions

We have synthesised a novel series of bis(isoquinolinylpyrazolate)palladium(II) metallomesogens $[Pd(pz^{R(n,n)iq})_2]$ (R(n,n) = $C_6H_3(OC_nH_{2n+1})_2$, n = 4, 6, 8, 10, 12, 14, 16, 18), exhibiting proton conduction in the tetragonal and hexagonal columnar mesophases. The melting points of the complexes determined by DSC could be confirmed by transitional features in the protonic conductivity σ' and capacitance C' vs T curves. The introduction of the isoquinolinyl group has favoured the thermal stability of the mesophases of these complexes, which are maintained stable up to elevated temperatures of 345 °C and higher. The complex with an intermediate chain length of n = 12 showed the highest protonic conductivity in the mesophase. It has been also demonstrated that the hexagonal columnar organisation of the mesophase favours the proton conduction with respect to the tetragonal columnar mesophase. The partial decomposition of the new Pd(II) complexes, which occur at very high temperatures, does not constitute a drawback for their potential applications in the liquid crystal

phase. The Pd(II) complex series presented in this work may be a promising step forward in the design of highly-stable proton conducting water-free electrolyte materials for potential application in PEM fuel cells.

Experimental

Starting materials

All commercial chemicals were purchased from Sigma-Aldrich, Alfa-Aesar or Maybridge and used without further purification. The 3-(3,5-bis(alkyloxy)phenyl)-5-(isoquinolin-3-yl)pyrazole ligands [$Hpz^{R(n,n)iq}$] were prepared as described in a previous work.[31]

Physical measurements

The elemental analyses (C, H, N) were carried out by the Microanalytical Service of Complutense University (validated range: %C 0.5 – 94.7, %H 0.5 – 7.6, %N 0.5 – 23.0). IR spectra were recorded on a FTIR Thermo Nicolet 200 spectrophotometer with samples as KBr pellets in the 4000 – 400 cm^{-1} region: w (weak), m (medium) and s (strong). ^1H and ^{13}C NMR, 2D COSY, selective 1D NOESY, ^1H-^{13}C HMQC and ^1H-^{13}C HMBC spectra were performed at room temperature on Bruker DPX-300 and Bruker AV-500 spectrophotometers (NMR Service of Complutense University) from solutions in $CDCl_3$. Chemical shifts δ are listed relative to Me_4Si using the signal of the deuterated solvent as a reference (7.26 and 77.0 ppm for ^1H and ^{13}C, respectively) and coupling constants *J* are in hertz. Multiplicities are indicated as s (singlet), d (doublet), t (triplet), q (quartet), qt (quintet), sx (sextuplet), m (multiplet), br (broad signal). The ^1H and ^{13}C chemical shifts are accurate to ±0.01 and ±0.1 ppm, respectively, and coupling constants to ±0.3 Hz.

Thermal studies were carried out by optical microscopy using an Olympus BX50 microscope equipped with a Linkam THMS 600 heating stage. The temperatures were assigned on the basis of optical observations with polarised light. Measurements of the transition temperatures and their associated enthalpies were performed using a Perkin Elmer Pyris 1 differential scanning calorimeter with the sample (1 – 4 mg) sealed hermetically in aluminium pans and with a heating or cooling rate of 10 K min^{-1}. The X-ray diffractograms at variable temperature were recorded on a Panalytical X'Pert PRO MPD diffractometer with Cu-Kα (1.54 Å) radiation in θ–θ configuration equipped with an Anton Paar HTK1200 heating stage (X-Ray Diffraction Service of Complutense University). TG experiments were recorded between 313 K (40 ºC) and 1237 K (964 ºC) on a Perkin-Elmer Pyris 1 TGA, with a heating rate of 10 K min^{-1} under N_2 atmosphere.

Dielectric measurements

The dielectric properties of the complexes in condensed form were measured by alternating current (AC) impedance spectroscopy using an Alpha Analyser integrated into the Novocontrol BDS 80. Measurements were performed at a frequency (*f*) range of 1 Hz – 10 MHz with 6 measurements points per frequency decade, using a 0.1 V applied AC voltage signal. The temperature (*T*) was varied between 160 K and the upper instrumental limit of 562 K (-113 ºC – 289 ºC) upon heating and cooling cycles. Dielectric data were taken under steady state conditions, where the selected *T* was stabilised for 3 - 10 minutes before taking impedance measurements over the full *f*-range. The temperature increments/reductions for taking impedance measurements were 20 K – 2 K steps, where the temperature was increased/decreased in smaller steps near the phase transitions. The complexes in the solid powder state (yellow colour) were placed between the polished electrodes of a custom-built stainless steel liquid cell with a high surface to thickness ratio.[49, 53] The cell was closed with a sapphire plate and placed inside the Novocontrol cryostat.

The electric response of the powder was obtained at selected temperatures for heating and cooling cycles in terms of the real and imaginary parts (Z', Z'') of the complex impedance $Z^* = Z' + iZ''$. The data were converted into the complex conductivity σ^* and capacitance C^* notations, $\sigma^* = \sigma' + i\sigma''$ and $C^* = C' - i\,C''$, using the standard conversions: $Z^* = (g\sigma^*)^{-1}$, and $Z^* = (i\omega C^*)^{-1}$, where *g* (in cm) is the geometrical factor given by electrode area divided by electrode distance, ω is the angular frequency. Due to experimental limitations *g* could only be estimated from the weight and density of the powder measured initially, and the measurement cell dimensions. Equivalent circuit fitting of the dielectric data was performed by using commercial Z-View software. The conductivity and permittivity values extracted from the equivalent circuit fits were plotted vs temperature, but only physically meaningful values with sufficiently low fitting errors (< 5%) were considered.

Synthesis of the palladium complexes $[Pd(pz^{R(n,n)iq})_2]$ 1-8

A solution of the corresponding isoquinolinylpyrazole ligand [$Hpz^{R(n,n)iq}$] (0.44 mmol) and a excess of 60% NaH (0.88 mmol, 35 mg) in 30 mL of CH_2Cl_2 was stirred for 30 min at room temperature. Then, 0.22 mmol (50 mg) of $[Pd(OOCCH_3)_2]$ previously dissolved in 5 mL of CH_2Cl_2 were added, and the reaction mixture was refluxed for 24 h. After this period, the solution was filtered over celite® and concentrated in vacuum. The addition of *ca.* 5 mL acetone yielded a yellow precipitate that was recrystallised in $CHCl_3$/acetone, filtered and dried under vacuum.

$[Pd(pz^{R(4,4)iq})_2]$ **(1)**. Yellow solid (37 %). Found: C, 66.5; H, 5.9; N, 9.0. $PdC_{52}N_6H_{56}O_4$ requires C, 66.8; H, 6.0; N, 9.0%. ν_{max}/cm^{-1} 2917-2849s ν(C-H)$_{aliphatic}$ and 1638-1594m ν(C=C + C=N). δ_H (300 MHz; $CDCl_3$; Me_4Si): 1.10 (12H, t, ^3J 7.2, CH_3), 1.57 (8H, sx, ^3J 7.3, CH_2), 1.83 (8H, qt, ^3J 6.7, CH_2), 3.83 (8H, t, ^3J 6.6, OCH_2), 6.03 (2H, s, 4'-H), 6.24 (2H, br, H_p), 6.44 (4H, br, H_o), 6.89 (2H, s, 4-H), 7.10 (2H, m, 7-H), 7.10 (2H, m, 5-H), 7.20 (2H, d, ^3J 8.0, 8-H), 7.39 (2H, m, 6-H), 10.20 (2H, s, 1-H).

$[Pd(pz^{R(6,6)iq})_2]$ **(2)**. Yellow solid (50 %). Found: C, 68.7; H, 6.8; N, 8.1. $PdC_{60}N_6H_{72}O_4$ requires C, 68.8; H, 6.9; N, 8.0%. ν_{max}/cm^{-1} 2929-2858m ν(C-H)$_{aliphatic}$ and 1639-1594s ν(C=C + C=N). δ_H (300 MHz; $CDCl_3$; Me_4Si): 1.00 (12H, t, ^3J 6.6, CH_3), 1.46 (24H, m, CH_2), 1.83 (8H, qt, ^3J 6.7, CH_2), 3.82 (8H, t, ^3J 6.7, OCH_2), 6.07 (2H, s, 4'-H), 6.25 (2H, br, H_p), 6.51 (4H, br, H_o),

6.93 (2H, s, 4-H), 7.10 (2H, m, 7-H), 7.18 (2H, d, ^{3}J 8.2, 5-H), 7.22 (2H, d, ^{3}J 8.2, 8-H), 7.43 (2H, m, 6-H), 10.29 (2H, s, 1-H).

[Pd(pz$^{R(8,8)iq}$)$_2$] **(3)**. Yellow solid (44 %). Found: C, 70.2; H, 7.4; N, 7.4. $PdC_{68}N_6H_{88}O_4$ requires C, 70.4; H, 7.6; N, 7.2%. ν_{max}/cm^{-1} 2923-2858m ν(C-H)$_{aliphatic}$ and 1638-1594s ν(C=C + C=N). δ_H (300 MHz; $CDCl_3$; Me_4Si): 0.96 (12H, t, ^{3}J 6.6, CH_3), 1.37 (40H, m, CH_2), 1.84 (8H, qt, ^{3}J 6.7, CH_2), 3.84 (8H, t, ^{3}J 6.8, OCH_2), 6.11 (2H, s, 4'-H), 6.27 (2H, t, ^{3}J 2.2, H_p), 6.56 (4H, d, ^{3}J 2.2, H_o), 6.96 (2H, s, 4-H), 7.14 (2H, m, 7-H), 7.21 (2H, d, ^{3}J 8.2, 5-H), 7.26 (2H, m, 8-H), 7.45 (2H, m, 6-H), 10.36 (2H, s, 1-H). δ_C (75.48 MHz; $CDCl_3$; Me_4Si): 14.2 (CH_3), 22.8 (CH_2), 26.3 (CH_2), 29.4 (CH_2), 29.7 (CH_2), 29.8 (CH_2), 32.0 (CH_2), 67.5 (OCH_2), 97.9 (C4'), 99.3 (C_P), 101.7 (C_O), 113.0 (C4), 125.2 (C10), 125.3 (C7), 125.8 (C5), 128.5 (C8), 130.8 (C6), 135.9 (C9), 136.8 (C_i), 145.3 (C3), 147.9 (C3'), 149.1 (C5'), 154.6 (C1), 159.5 (C_m).

[Pd(pz$^{R(10,10)iq}$)$_2$] **(4)**. Yellow solid (40 %). Found: C, 71.6; H, 8.0; N, 6.6. $PdC_{76}N_6H_{104}O_4$ requires C, 71.8; H, 8.2; N, 6.6%. ν_{max}/cm^{-1} 2919-2850s ν(C-H)$_{aliphatic}$ and 1637-1593s ν(C=C + C=N). δ_H (300 MHz; $CDCl_3$; Me_4Si): 0.93 (12H, t, ^{3}J 6.9, CH_3), 1.33 (56H, m, CH_2), 1.84 (8H, qt, ^{3}J 6.8, CH_2), 3.85 (8H, t, ^{3}J 6.7, OCH_2), 6.13 (2H, s, 4'-H), 6.28 (2H, t, ^{3}J 2.2, H_p), 6.58 (4H, d, ^{3}J 2.2, H_o), 6.99 (2H, s, 4-H), 7.16 (2H, m, 7-H), 7.23 (2H, d, ^{3}J 8.5, 5-H), 7.30 (2H, d, ^{3}J 8.1, 8-H), 7.47 (2H, m, 6-H), 10.39 (2H, s, 1-H).

[Pd(pz$^{R(12,12)iq}$)$_2$] **(5)**. Yellow solid (51 %). Found: C, 71.6; H, 8.4; N, 6.0. $PdC_{84}N_6H_{120}O_4{\cdot}0.2CHCl_3$ requires C, 71.8; H, 8.6; N, 6.0%. ν_{max}/cm^{-1} 2919-2850s ν(C-H)$_{aliphatic}$ and 1638-1593s ν(C=C + C=N). δ_H (300 MHz; $CDCl_3$; Me_4Si): 0.91 (12H, t, ^{3}J 7.1, CH_3), 1.31 (72H, m, CH_2), 1.84 (8H, br, CH_2), 3.88 (8H, br, OCH_2), 6.22 (2H, s, 4'-H), 6.30 (2H, br, H_p), 6.62 (4H, br, H_o), 7.10 (2H, s, 4-H), 7.19 (2H, m, 7-H), 7.26 (2H, br, 5-H), 7.36 (2H, br, 8-H), 7.50 (2H, m, 6-H), 10.44 (2H, s, 1-H).

[Pd(pz$^{R(14,14)iq}$)$_2$] **(6)**. Yellow solid (50 %). Found: C, 73.7; H, 8.7; N, 5.7. $PdC_{92}N_6H_{136}O_4$ requires C, 73.8; H, 9.1; N, 5.6%. ν_{max}/cm^{-1} 2917-2850s ν(C-H)$_{aliphatic}$ and 1638-1594s ν(C=C + C=N). δ_H (300 MHz; $CDCl_3$; Me_4Si): 0.91 (12H, t, ^{3}J 7.0, CH_3), 1.32 (88H, m, CH_2), 1.86 (8H, qt, ^{3}J 6.8, CH_2), 3.88 (8H, br, OCH_2), 6.23 (2H, s, 4'-H), 6.30 (2H, br, H_p), 6.62 (4H, br, H_o), 7.09 (2H, s, 4-H), 7.19 (2H, m, 7-H), 7.30 (2H, br, 5-H), 7.36 (2H, d, ^{3}J 7.7, 8-H), 7.50 (2H, m, 6-H), 10.43 (2H, s, 1-H).

[Pd(pz$^{R(16,16)iq}$)$_2$] **(7)**. Yellow solid (57 %). Found: C, 73.9; H, 9.2; N, 5.1. $PdC_{100}N_6H_{152}O_4{\cdot}0.2CHCl_3$ requires C, 73.7; H, 9.4; N, 5.2%. ν_{max}/cm^{-1} 2918-2850s ν(C-H)$_{aliphatic}$ and 1638-1594s ν(C=C + C=N). δ_H (300 MHz; $CDCl_3$; Me_4Si): 0.89 (12H, t, ^{3}J 7.0, CH_3), 1.28 (104H, m, CH_2), 1.86 (8H, qt, ^{3}J 6.9, CH_2), 3.89 (8H, t, ^{3}J 6.7, OCH_2), 6.26 (2H, s, 4'-H), 6.31 (2H, br, H_p), 6.66 (4H, br, H_o), 7.12 (2H, s, 4-H), 7.22 (2H, m, 7-H), 7.31 (2H, d, ^{3}J 8.2, 5-H), 7.41 (2H, d, ^{3}J 8.1, 8-H), 7.51 (2H, m, 6-H), 10.50 (2H, s, 1-H).

[Pd(pz$^{R(18,18)iq}$)$_2$] **(8)**. Yellow solid (60 %). Found: C, 75.2; H, 9.4; N, 5.0. $PdC_{108}N_6H_{168}O_4$ requires C, 75.4; H, 9.8; N, 4.9%. ν_{max}/cm^{-1} 2918-2850s ν(C-H)$_{aliphatic}$ and 1638-1595m ν(C=C + C=N). δ_H (300 MHz; $CDCl_3$; Me_4Si): 0.88 (12H, t, ^{3}J 7.1, CH_3), 1.26 (120H, m, CH_2), 1.88 (8H, br, CH_2), 3.98 (8H, br, OCH_2), 6.37 (2H, s, 4'-H), 6.51 (2H, br, H_p), 6.83 (4H, br, H_o), 7.26 (2H, s, 4-H), 7.37 (2H, br, 7-H), 7.47 (2H, br, 5-H), 7.62 (2H, br, 8-H), 7.62 (2H, br, 6-H), 10.78 (2H, s, 1-H).

Acknowledgements

View Article Online
DOI: 10.1039/C6DT03521C

M. Cano thanks the Spanish Ministerio de Economía y Competitividad (project CTQ2015-63858-P (MINECO/FEDER)) for funding. C. Cuerva is grateful to the Programa de Financiación de Universidad Complutense de Madrid-Santander Universidades (Spain), for his predoctoral contract. The authors wish to express their gratitude to Alberto Rivera-Calzada, Carlos León and Jacobo Santamaría for allowing use and assistance with the dielectric spectroscopy.

Notes and references

1. B. R. Kaafarani, *Chem. Mater.* , 2011, **23**, 378.
2. S. Belviso, M. Amati, R. Rossano, A. Crispini and F. Lelj, *Dalton Trans.*, 2015, **44**, 2191.
3. S. Sergeyev, W. Pisula and Y. H. Geerts, *Chem. Soc. Rev.*, 2007, **36**, 1902.
4. T. Wöhrle, I. Wurzbach, J. Kirres, A. Kostidou, N. Kapernaum, J. Litterscheidt, J. C. Haenle, P. Staffeld, A. Baro, F. Giesselmann and S. Laschat, *Chem. Rev.*, 2016, **116**, 1139.
5. L. A. Tatum, C. J. Johnson, A. A. P. Fernando, B. C. Ruch, K. K. Barakoti, M. A. Alpuche-Aviles and B. T. King, *Chem. Sci.*, 2012, **3**, 3261.
6. D. Adam, F. Closs, T. Frey, D. Funhoff, D. Haarer, P. Schuhmacher and K. Siemensmeyer, *Phys. Rev. Lett.*, 1993, **70**, 457.
7. L. Schmidt-Mende, A. Fechtenkötter, K. Müllen, E. Moons, R. H. Friend and J. D. MacKenzie, *Science*, 2001, **293**, 1119.
8. I. Seguy, P. Jolinat, P. Destruel, J. Farenc, R. Mamy, H. Bock, J. Ip and T. P. Nguyen, *J. Appl. Phys.*, 2001, **89**, 5442.
9. O. Kasdorf, J. Vollbrecht, B. Ohms, U. Hilleringmann, H. Bock and H.-S. Kitzerow, *Int. J. Energy Res.*, 2014, **38**, 452.
10. J. Eccher, W. Zajaczkowski, G. C. Faria, H. Bock, H. von Seggern, W. Pisula and I. H. Bechtold, *ACS Appl. Mater. Interfaces*, 2015, **7**, 16374.
11. I. O. Shklyarevskiy, P. Jonkheijm, N. Stutzmann, D. Wasserberg, H. J. Wondergem, P. C. M. Christianen, A. P. H. J. Schenning, D. M. de Leeuw, Ž. Tomović, J. Wu, K. Müllen and J. C. Maan, *J. Am. Chem. Soc.*, 2005, **127**, 16233.
12. H. Iino, T. Usui and J.-i. Hanna, *Nat. Commun.*, 2015, **6**.
13. X. Guo, S. Xiao, M. Myers, Q. Miao, M. L. Steigerwald and C. Nuckolls, *Proc. Natl. Acad. Sci. U S A.*, 2009, **106**, 691.
14. W. W. H. Wong, J. Subbiah, S. R. Puniredd, B. Purushothaman, W. Pisula, N. Kirby, K. Mullen, D. J. Jones and A. B. Holmes, *J. Mater. Chem.*, 2012, **22**, 21131.
15. Y. Shi, L. Tan and Y. Chen, *ACS Appl. Mater. Interfaces*, 2014, **6**, 17848.
16. Q. Zheng, G. Fang, W. Bai, N. Sun, P. Qin, X. Fan, F. Cheng, L. Yuan and X. Zhao, *Sol. Energ. Mat. Sol. Cells*, 2011, **95**, 2200.
17. X. Chen, L. Chen and Y. Chen, *RSC Adv.*, 2014, **4**, 3627-3632.
18. M. Yoshio, T. Mukai, H. Ohno and T. Kato, *J. Am. Chem. Soc.*, 2004, **126**, 994.
19. H. Shimura, M. Yoshio, K. Hoshino, T. Mukai, H. Ohno and T. Kato, *J. Am. Chem. Soc.*, 2008, **130**, 1759.
20. M. Yoshio, T. Kagata, K. Hoshino, T. Mukai, H. Ohno and T. Kato, *J. Am. Chem. Soc.*, 2006, **128**, 5570.
21. M. Yoshio, T. Mukai, H. Ohno and T. Kato, in *Ionic Liquids IV*, American Chemical Society, 2007, vol. 975, ch. 11, pp. 161-171.
22. B. Soberats, M. Yoshio, T. Ichikawa, H. Ohno and T. Kato, *J. Mater. Chem. A*, 2015, **3**, 11232.

23. S. Ueda, J. Kagimoto, T. Ichikawa, T. Kato and H. Ohno, *Adv. Mater.*, 2011, **23**, 3071.
24. A. Yamashita, M. Yoshio, B. Soberats, H. Ohno and T. Kato, *J. Mater. Chem. A*, 2015, **3**, 22656.
25. D. Basak, S. Christensen, S. K. Surampudi, C. Versek, D. T. Toscano, M. T. Tuominen, R. C. Hayward and D. Venkataraman, *Chem. Commun.*, 2011, **47**, 5566.
26. S. Tan, B. Wei, T. Liang, X. Yang and Y. Wu, *RSC Adv.*, 2016, **6**, 34038.
27. T. Liang, Y. Wu, S. Tan and C. Wang, *J. App. Polym. Sci.*, 2014, **131**, 40382.
28. C. Cuerva, J. A. Campo, P. Ovejero, M. R. Torres and M. Cano, *Dalton Trans.*, 2014, **43**, 8849.
29. C. Cuerva, J. A. Campo, P. Ovejero, M. R. Torres, E. Oliveira, S. M. Santos, C. Lodeiro and M. Cano, *J. Mater. Chem. C*, 2014, **2**, 9167.
30. C. Cuerva, J. A. Campo, M. Cano, B. Arredondo, B. Romero, E. Oton and J. M. Oton, *New J. Chem.*, 2015, **39**, 8467.
31. C. Cuerva, J. A. Campo, M. Cano and C. Lodeiro, *Chem. Eur. J.*, 2016, **22**, 10168.
32. H.-Y. Ku, B. Tong, Y. Chi, H.-C. Kao, C.-C. Yeh, C.-H. Chang and G.-H. Lee, *Dalton Trans.*, 2015, **44**, 8552.
33. S.-Y. Chang, J. Kavitha, J.-Y. Hung, Y. Chi, Y.-M. Cheng, E. Y. Li, P.-T. Chou, G.-H. Lee and A. J. Carty, *Inor. Chem.*, 2007, **46**, 7064.
34. J. Kavitha, S. Y. Chang, Y. Chi, J. K. Yu, Y. H. Hu, P. T. Chou, S. M. Peng, G. H. Lee, Y. T. Tao, C. H. Chien and A. J. Carty, *Adv. Funct. Mater.*, 2005, **15**, 223.
35. T. D. Choudhury, N. V. S. Rao, R. Tenent, J. Blackburn, B. Gregg and I. I. Smalyukh, *J. Phys. Chem. B*, 2011, **115**, 609.
36. E. Pouzet, V. D. Cupere, C. Heintz, J. W. Andreasen, D. W. Breiby, M. M. Nielsen, P. Viville, R. Lazzaroni, G. Gbabode and Y. H. Geerts, *J. Phys. Chem. C*, 2009, **113**, 14398.
37. K. Ohta, T. Watanabe, H. Hasebe, Y. Morizumi, T. Fujimoto, I. Yamamoto, D. Lelièvre and J. Simon, *Mol. Cryst. Liq. Cryst.*, 1991, **196**, 13.
38. T. Komatsu, K. Ohta, T. Watanabe, H. Ikemoto, T. Fujimoto and I. Yamamoto, *J. Mater. Chem.*, 1994, **4**, 537.
39. B. Chen, U. Baumeister, G. Pelzl, M. K. Das, X. Zeng, G. Ungar and C. Tschierske, *J. Am. Chem. Soc.*, 2005, **127**, 16578.
40. J. T. S. Irvine, D. C. Sinclair and A. R. West, *Adv. Mater.*, 1990, **2**, 132.
41. M. A. Frechero, M. Rocci, G. Sánchez-Santolino, A. Kumar, J. Salafranca, R. Schmidt, M. R. Díaz-Guillén, O. J. Durá, A. Rivera-Calzada, R. Mishra, S. Jesse, S. T. Pantelides, S. V. Kalinin, M. Varela, S. J. Pennycook, J. Santamaria and C. Leon, *Sci. Rep.*, 2015, **5**, 17229.
42. K. Funke and R. Hoppe, *Solid State Ionics*, 1990, **40**, 200.
43. B. A. Boukamp, *Solid State Ionics*, 2004, **169**, 65.
44. R. Ameloot, M. Aubrey, B. M. Wiers, A. P. Gómora-Figueroa, S. N. Patel, N. P. Balsara and J. R. Long, *Chem. Eur. J.*, 2013, **19**, 5533.
45. S. Kim, M. Hirayama, S. Taminato and R. Kanno, *Dalton Trans.*, 2013, **42**, 13112.
46. S. Mudenda and G. M. Kale, *J. Mater. Chem. A*, 2015, **3**, 12268-12275.
47. E. Barsukov and J. Macdonald, *Impedance Spectroscopy: Theory, Experiment and Applications*, John Wiley & Sons Inc., Hoboken, 2005.
48. F. Preishuber-Pflugl and M. Wilkening, *Dalton Trans.*, 2016, **45**, 8675.
49. C. Cuerva, J. A. Campo, M. Cano, J. Sanz, I. Sobrados, V. Diez-Gómez, A. Rivera-Calzada and R. Schmidt, *Inorg. Chem.*, 2016, **55**, 6995.
50. A. K. Jonscher, *Nature*, 1977, **267**, 673.
51. *Proton Conductors: Solids, Membranes and Gels - Materials and Devices*, Cambridge, Victoria, Australia, 2008.
52. J. Prado-Gonjal, R. Schmidt, J. Espíndola-Canuto, P. Ramos-Alvarez and E. Morán, *J. Power Sources*, 2012, **209**, 163-171.
53. C. Gainaru, A. Rivera, S. Putselyk, G. Eska and E. A. Rössler, *Phys. Rev. B*, 2005, **72**, 174203.

View Article Online
DOI: 10.1039/C6DT03521C

Nanostructured discotic Pd(II) metallomesogens as one-dimensional proton conductors

Cristián Cuerva,[a] José A. Campo,[a] Mercedes Cano*[a] and Rainer Schmidt*[b]

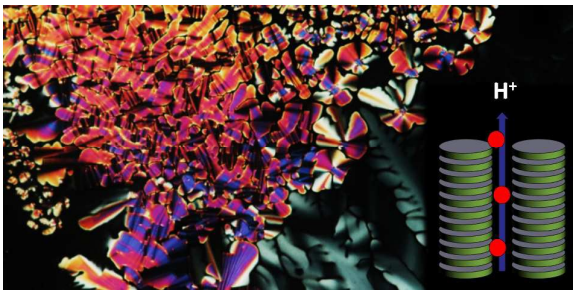

Bis(isoquinolinylpyrazolate) Pd(II) metallomesogens may be a promising step forward in the design of highly-stable proton conducting water-free electrolyte materials.